RSC Advances

ROYAL SOCIETY OF CHEMISTRY

www.rsc.org/advances

Synthesis of Ag/ZnO/C plasmonic photocatalyst with enhanced adsorption capacity and photocatalytic activity to antibiotic

Jinjuan Xue[‡, a], Shuaishuai Ma[‡, a], Yuming Zhou[*, a], Zewu Zhang[a] and Ping Jiang[b]

[a] School of Chemistry and Chemical Engineering, Southeast University, Nanjing 211189, P. R. China

[b] Xuchuan Chemical (Suzhou) Co., Ltd, Taicang 215434, P. R. China

Abstract Novel Ag/ZnO/C plasmonic photocatalyst was synthesized via a facile calcination and photodeposition route. The samples were characterized by X-ray diffraction (XRD), energy dispersive X-ray spectroscopy (EDS), transmission electron microscopy (TEM) and ultraviolet-visible diffuse reflectance spectroscopy (UV-vis DRS). The results indicated that the Ag and ZnO nanoparticles sized 5-10 nm were uniformly dispersed on the surface of the carbonaceous layers in Ag/ZnO/C composites. The adsorption capacity and photocatalytic activity were investigated by adsorption and photocatalytic degradation of tetracycline hydrochloride (TC-HCl) in aqueous solution. The results showed that the obtained Ag/ZnO/C sample exhibited higher adsorption capacity and enhanced UV and visible light driven photocatalytic activity to TC-HCl compared to ZnO/C and pure ZnO. With the presence of the Ag nanoparticles and carbonaceous layers incorporating in the structure, the Ag/ZnO/C composites can make use of not only the UV region of sunlight, but also the visible region and efficiently promote photogenerated electron separation and transportation as well as generate more active reaction sites, which synergistically facilitate the photocatalysis process.

[*] Corresponding author. Tel.: +86 25 52090617; fax: +86 25 52090617.
E-mail address: ymzhou@seu.edu.cn (Yuming Zhou).
‡ J.J. Xue and S.S. Ma contributed equally to this work.

Our present work provides a simple and new pathway into the design of ZnO-based catalyst response to both UV and visible light and promotes their practical application in various environmental and energy issues driven by solar light.

Introduction

In decades, pharmaceutical compounds that cause contamination of the environment have aroused worldwide attention. Among all the pharmaceutical compounds contaminants, antibiotics occupy an important place due to their high consumption rate in both veterinary and human medicine.[1] Antibiotic residues in the environment may induce antibiotic resistant bacteria and affect microbes in the environment.[2-4] Therefore, they have the potential to negatively affect either aquatic or terrestrial ecosystems, even in low concentrations.[5, 6] In comparison with other conventional techniques such as activated carbon adsorption, microbial degradation and electrolysis to deal with the antibiotic residues, photocatalysis appears to be a green and efficiency technology and effective photocatalysts have been developed to degrade the antibiotic residues.[7] For example, photocatalytic degradation of ceftiofur sodium in the presence of Au-TiO_2 under UV-visible light,[8] degradation of antibiotic norfloxacin in aqueous solution by visible-light-mediated C-TiO_2 photocatalysis,[9] aqueous tetracycline degradation by non-thermal plasma combined with nano-TiO_2,[10] and so on. Currently, zinc oxide (ZnO) is one of the most studied photocatalysts owing to its physical and chemical stability, high catalytic activity, low cost, environmental friendliness and easy of availability.[11, 12] However, ZnO is a wide band gap (3.37 eV) semiconductor with inevitable shortcomings for photocatalysis-based applications, especially the poor utilization of solar energy and the short diffusion length of a photogenerated electron-hole pair are the two major factors limiting the

further improvement of photocatalytic efficiency.[13] Therefore, it is necessary to develop new strategies for a more efficient ZnO-based photocatalyst that could utilize the visible portion of the sunlight and facilitate electron separation. To date, several efforts have been devoted to reducing the recombination of photogenerated electron-hole pairs and improving the utilization of solar light of ZnO, such as special nanocrystal microstructures and morphologies design,[14, 15] doping elements,[16, 17] deposition of metals,[18, 19] combining ZnO with another semiconductor,[20-22] or hybridizing ZnO with carbon materials.[23-25] In particular, carbonaceous materials have been widely used as ideal electron pathways due to their good conductivity. Some results have demonstrated that carbonaceous materials could efficiently capture and transport of photogenerated electrons because of their highly conductive activity.[13, 25-27] If the nanostructured ZnO is modified by carbonaceous materials, the good properties of ZnO and carbonaceous materials will be integrated into the hybrids, which are advantageous to overcoming some intrinsic defects of ZnO. In the first, the introduction of carbonaceous materials on ZnO will make the latter more environmentally safe because of that carbonaceous materials are more inert than ZnO and are less affected in physiological conditions. Second, ZnO is an amphoteric compound and easily suffers from the corrosion of acid and base; the presence of carbonaceous materials could protect ZnO from the destruction. Finally, amorphous carbonaceous materials and other related materials are low work function materials, and hence the combination of them with ZnO will modify the optical and electronic properties of ZnO. Based on this, many kinds of ZnO-carbon composites have been developed to improve the photocatalysis property of ZnO, which will not only reduce electron-hole recombination, but also enlarge the absorption band of pure ZnO to the visible

region.[28-30]

In addition to this, noble metals, such as gold (Au) and silver (Ag), possess an additional ability to absorb visible light due to the existence of surface plasmon resonance (SPR),[31] so the introduction of Au or Ag could entitle the novel metal-ZnO composites visible light response ability. Besides, the noble metal-ZnO composites could effectively restrain the recombination of electron-hole pairs by a fast transfer of photogenerated electrons onto Ag or Au.[32] These methods all give a notable improvement on the photocatalysis property of ZnO.

In this paper, we demonstrate a simple calcination and photodeposition method for fabricating Ag/ZnO/C plasmonic photocatalyst. This method is facile, mild and eco-friendly. The prepared samples were well characterized and the results indicated that ZnO and Ag nanoparticles were individually and uniformly distributed on the carbonaceous layers. The as-prepared Ag/ZnO/C composites exhibited outstanding adsorption capacity and photocatalytic activity for adsorption and degradation of TC-HCl (a typical antibiotic). Furthermore, two different photocatalytic mechanisms of Ag/ZnO/C plasmonic photocatalyst under UV and visible-light irradiation were proposed and discussed.

Experimental section

Materials

Silver nitrate ($AgNO_3$), ethanol, zinc citrate dihydrate and tetracycline hydrochloride (TC-HCl) were purchased from Aladdin Chemical Regent Co., Ltd. (Shanghai, China). All the reagents in this experiment are analytically pure and used without further purification.

Synthesis of ZnO/C composites and bare ZnO nanoparticles

ZnO/C composites were synthesis according to the method in our previous work.[33] In a typical procedure, the precursor zinc citrate dehydrate (2.0 g) was placed into quartz boats and heat-treated in a tube furnace at 550 ^{o}C under nitrogen atmosphere for 3 h with a heating rate of 10 ^{o}C/min. The black-colored product was collected and marked as ZnO/C(550N). For comparison, bare ZnO nanoparticles were prepared by the same method, except for that the calcination atmospheric condition changed to air atmosphere. The obtained sample was marked as ZnO(550A).

Preparation of Ag/ZnO/C plasmonic photocatalyst

Typically, 0.45 g of ZnO/C(550N) was dispersed in 100 mL of ethanol by sonication for 30 min to form a uniform suspension. Subsequently, 1 mL of $AgNO_3$ ethanol solution (0.1431 g $AgNO_3$ in 20 mL ethanol) was added to the above suspension. The mixture was stirred for 1 h in the absence of light, then irradiated with a 250W high-pressure mercury lamp (λ = 365 nm) for 30 min under nitrogen atmosphere with stirring. The resulting product was collected by centrifugation, then washed with deionized water and dried under vacuum to obtain the Ag/ZnO/C plasmonic photocatalyst and the Ag content is 1 wt%.

Sample characterizations

X-ray diffraction (XRD) measurement was carried out using a SmartLab XRD spectrometer (Rigaku) with Cu Kα radiation in the range of 10-70° (2θ). Energy dispersive X-ray spectroscopy (EDS) was used to analyze the composition of samples. Transmission electron microscopy (TEM; JEM-1230) and high resolution TEM (HRTEM) were used to characterize the morphologies of the products. Thermogravimetric analysis (TGA) was performed on a Mettler-Toledo TGA/SDTA851e. X-ray photoelectron spectroscopy (XPS)

measurement was performed with a Kratos Axis Ultra DLD spectrometer equipped with a monochromatic Al Kα X-ray source (1486.6 eV). The nitrogen adsorption and desorption isotherms were measured at 77 K on an ASAP 2020 (Micromertics USA). UV-vis diffuse reflectance spectra (DRS) of the samples were recorded on a UV-vis spectrophotometer (UV-3600, Shimadzu) with an integrating sphere attachment. PL spectra were measured using room temperature photoluminescence with a 325 nm He-Cd laser excitation wavelength (Shimadzu RF-5301).

Adsorption and photocatalytic degradation of TC-HCl

100 mg Ag/ZnO/C plasmonic photocatalyst was added into 100 mL of 20 mg/L tetracycline hydrochloride (TC-HCl) aqueous solution. A 250 W UV lamp with maximum emission at 365 nm was used as UV light source and a 500 W xenon lamp with a UV cut-off filter with $\lambda > 400$ nm was used as the visible light source. Prior to light irradiation, the suspension was stirred for 40 min in the dark for adsorption/desorption equilibrium between the photocatalyst and TC-HCl. Subsequently, the above suspension was irradiated in a photochemical chamber under continuously stirring with reflux water to keep its temperature constant. Samples were taken at pre-selected time intervals using a syringe and filtered through a 0.45μm PTFE syringe filter to get clear liquid. The quantitative determination of TC-HCl was performed by measuring its intensity of the characteristic absorption peak at 355 nm with a UV-vis spectrophotometer. Comparative experiments of degradation TC-HCl by ZnO/C(550N) and ZnO(550A) samples were also carried out.

Results and discussion

Structure and Morphology

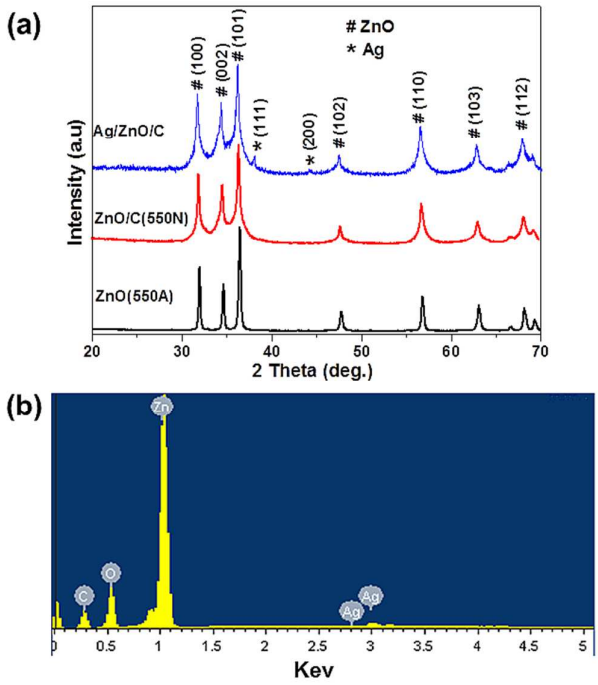

Fig. 1 XRD patterns of (a) ZnO(550A), ZnO/C(550N) and Ag/ZnO/C composites, and EDS spectrum of (b) the Ag/ZnO/C.

Fig. 1 (a) depicts the XRD patterns of ZnO(550A), ZnO/C(550N) and Ag/ZnO/C composites. It can be found that all the diffraction peaks in the pattern of ZnO(550A) can be indexed a hexagonal phase of wurtzite-type ZnO with lattice constants a = 3.249 Å and c = 5.206 Å, in accordance with the standard date (JCPDS Card No. 65-3411). All of the diffraction peaks of ZnO/C(550N) composites also can be indexed to ZnO in a hexagonal structure. The difference between the XRD patterns of ZnO/C(550N) and ZnO(550A) is that the noise level of the former is higher, which is resulted from the scattering of X-rays caused by the amorphous carbon layers. In contrast, the Ag/ZnO/C sample exhibited additional peaks at 38^{o} and 44.2^{o}, which can be indexed to the (111) and (200) planes of Ag, respectively (JCPDS Card No. 65-2871).The EDS pattern (Fig. 1 (b)) further demonstrated that the

Ag/ZnO/C sample was composed of Ag, Zn, O, and C atoms.

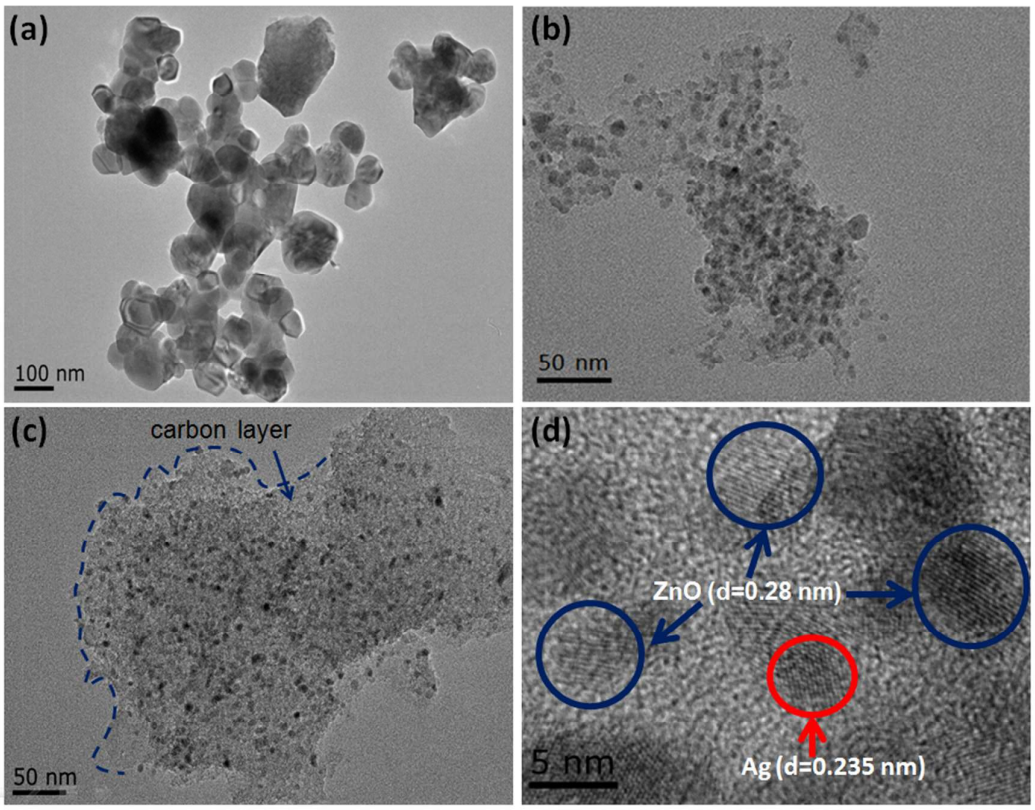

Fig. 2 Typical TEM images (a) ZnO(550A), (b) ZnO/C(550N), (c) Ag/ZnO/C composites and HRTEM (d) image of the as-prepared Ag/ZnO/C composites.

The morphologies of ZnO(550A), ZnO/C(550N), Ag/ZnO/C composites were investigated by transmission electron microscopy (TEM) and high resolution TEM (HRTEM) as shown in Fig. 2. It can be found in Fig. 2 (a) that the microstructure of the ZnO(550A) sample was composed of irregular nanoparticles with diameter of about 50-100 nm. Fig. 2 (b) and Fig. 2 (c) show the typical TEM images of ZnO/C(550N) and Ag/ZnO/C composites, respectively. As can be seen from Fig 2 (b and c), the obvious edge indicated that carbonaceous material existed in the composites was in the form of layers and the ZnO and Ag nanoparticles sized 5-10 nm were densely deposited on the carbonaceous layers. The carbon layers provides good support for the densely distributed ZnO and Ag nanoparticles,

implying that the ZnO, Ag and carbonaceous layers were integrated with an intimate interfacial contact by the calcination and photodeposition process. Moreover, the transparency of the carbon layers also suggested that the ZnO/C(550N) and Ag/ZnO/C composites had a high porosity. From the HRTEM image in Fig. 2(d), the resolved interplanar distance of 0.28 nm agrees well with the lattice spacing of the (100) plane of the wurtzite ZnO and the interplanar distance of 0.235 nm is the d-spacing value of the (111) plane of metallic Ag, which is consistent with the XRD and EDS results in Fig. 1.

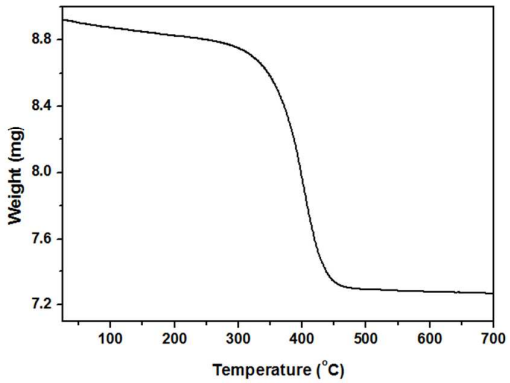

Fig. 3 The TGA spectrum of the ZnO/C(550N) sample.

Thermogravimetric analysis (TGA) was applied to determine the carbon content in the composites. On account of that Ag will have an oxidation and reduction process in the TGA procedure, ZnO/C(550N) was used as the analysis sample. As shown in Fig. 3, two main weight loss events were observed in the TGA curve. The first one that occurred between room temperature and 150 ^{o}C with a weight loss of about 1 wt% due to the desorption of physically adsorbed water from the sample. Another major weight loss commenced at around 300 °C and was completed at 640 °C, which can be attributed to the oxidation of carbon. After calculation, the carbon content of ZnO/C(550N) was 17.4 wt %. Since the Ag content is very low in the Ag/ZnO/C composites, we considered that the carbon content in the Ag/ZnO/C composites is

close to that in the ZnO/C(550N) sample.

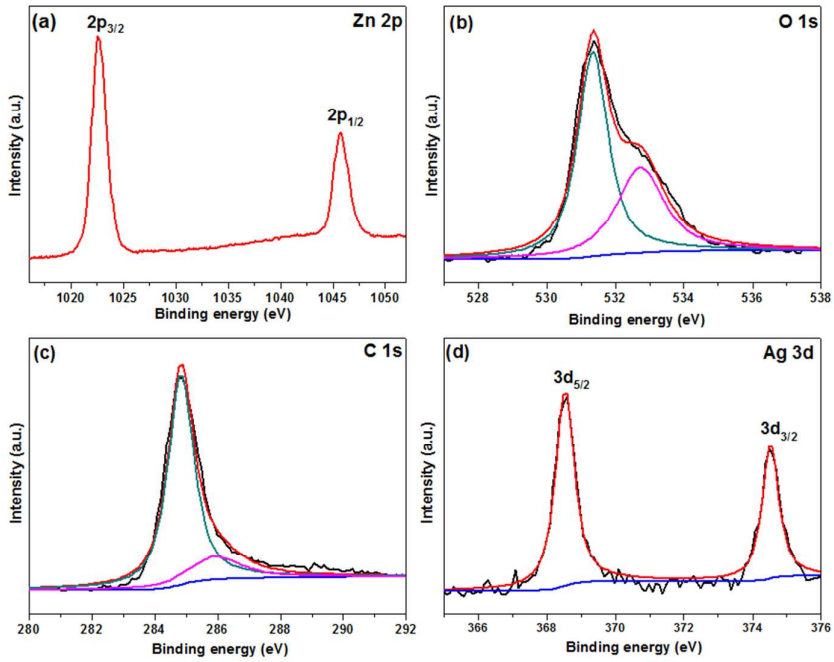

Fig. 4 XPS spectra of (a) Zn 2p, (b) O 1s, (c) C 1s and (d) Ag 3d of the as-prepared Ag/ZnO/C composites.

More detailed information regarding the element chemical status of the as-prepared Ag/ZnO/C composites was investigated by X-ray photoelectron spectroscopy (XPS), as shown in Fig. 4. It can be seen from Fig.4(a) that the Zn 2p spectrum contains two peaks centered at 1022.6 and 1045.8 eV, assigned to Zn $2p_{3/2}$ and $2p_{1/2}$, respectively. The binding energy distance between these two bands is 23.2 eV, which is within the standard reference value of ZnO and indicates that the Zn ions in the composites are of +2 states.[34, 35] In the O 1s XPS spectrum of Fig. 4(b), one peak located at 531.4 eV is assigned to O^{2-} ions in the Zn-O bonds of the wurtzite ZnO structure,[36] while another peak located at 533.0 eV could be related to OH group absorbed onto the surface of the composites.[37] The C 1s spectrum of Fig. 4(c) can be deconvoluted into two peaks with binding energy values of 284.9 and 286.1 eV, and the two peaks are assigned to sp^2 hybridized carbon and the oxygen bound species C-O, respectively.[38, 39] Nevertheless, no C 1s peak at around 282.5 eV attributed to Zn-C bonds[40] was observed, indicating that carbon

does not enter the ZnO-phase and ZnO nanoparticles attached to the surface of carbonaceous layers via Zn-O-C bonds. The Ag 3d spectrum in Fig. 4(d) shows two peaks centered at 368.3 and 374.3 eV, which can be ascribed to Ag $3d_{5/2}$ and Ag $3d_{3/2}$, respectively. According to the previous reports, we have learned that metallic Ag 3d peaks are centered at 367.9 and 373.9 eV, while the Ag iron exhibits two peaks at 369.4 and 375.6 eV.[41, 42] Therefore, our experimental data indicate that a small amount of Ag^+ is present on the surface of Ag nanoparticles, which is probably due to the electrons transfer from metallic Ag to carbonaceous layers as the formation of Ag/C heterostructure.[32, 43]

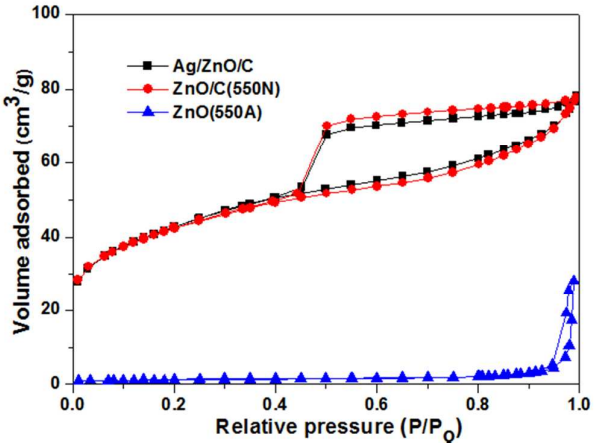

Fig. 5 N_2 adsorption-desorption isotherm of the as-prepared ZnO(550A), ZnO/C(550N) and Ag/ZnO/C composites.

Sample	Surface area (m^2/g)	pore volume (cm^3/g)	Mean pore size (nm)
ZnO(550A)	4.24	0.0436	41.10
ZnO/C(550N)	147.20	0.1202	3.22
Ag/ZnO/C	151.73	0.1208	3.18

Table 1 Parameters obtained from the nitrogen desorption isotherm experiments.

In Fig. 5, the corresponding nitrogen adsorption-desorption isotherm of ZnO(550A) exhibits type IV isotherm shape according to the IUPAC classification, while the nitrogen adsorption-desorption isotherms of ZnO/C(550N) and Ag/ZnO/C composites exhibited type

IV-like isotherms with H2 hysteresis loops according to IUPAC, which are associated with capillary condensation taking place in mesopores.[39] The parameters obtained from nitrogen desorption isotherms of different samples are given in Table 1. The calculated BET surface area of ZnO/C(550N) and Ag/ZnO/C composites are 147.20 m^2/g and 151.73 m^2/g, respectively, which are much higher than that of ZnO(550A) (4.24 m^2/g). The porous carbon layers and the small size of the deposited ZnO and Ag nanoparticles both might contribute to the improved surface area of the composites, then facilitate the photolysis of the composites due to the improved adsorbability.

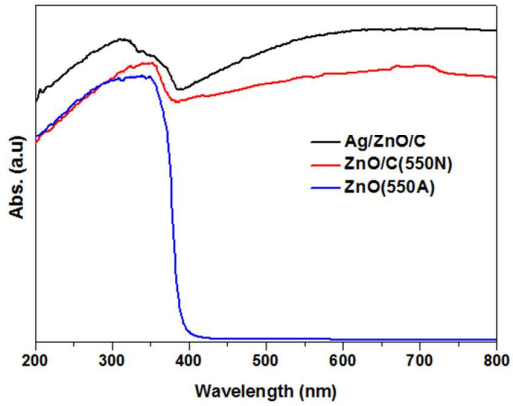

Fig. 6 UV/Vis diffuse reflectance spectra of ZnO(550A), ZnO/C(550N) and Ag/ZnO/C composites.

The optical absorption plays an important role in the photocatalysis, especially in the visible-light photodegradation of contaminants.[44, 45] The optical absorption properties of ZnO(550A), ZnO/C(550N) and Ag/ZnO/C composites measured with UV/Vis diffuse reflectance spectroscopy (DRS) are demonstrated in Fig. 6. As can be seen, ZnO(550A) shows a steep adsorption edge located at 380 nm and an absorption band lower than 380 nm (UV region). Compared to pure ZnO, ZnO/C(550N) displays strong capability of light absorption in both UV and visible light range of 200-800 nm. It is resulted from that the carbon layers incorporated in the composites modified the optical properties of ZnO, which is

similar to carbon nanotubes-ZnO and C-doped TiO_2 studies.[28, 46] Furthermore, the Ag/ZnO/C sample exhibits more intense absorption than that of ZnO/C(550N) due to the surface plasmon resonance absorption of Ag nanoparticles.[47] As a result of this enlarged light absorption range and intensity, Ag/ZnO/C plasmonic photocatalyst is expected to achieve more efficient utilization of the solar spectrum and shows enhanced photocatalytic activity.

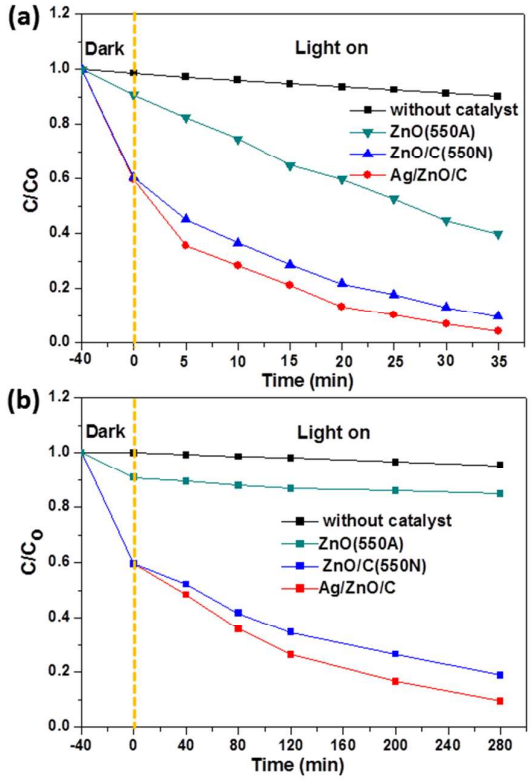

Fig. 7 Photocatalytic activities of the as-prepared ZnO(550A), ZnO/C(550N) and Ag/ZnO/C composites for degradation of TC-HCl: (a) under UV irradiation; (b) under visible light irradiation.

Photocatalytic Activity

Fig. 7 presents the photocatalytic activities of the as-prepared ZnO(550A), ZnO/C(550N) and Ag/ZnO/C samples under UV and visible light irradiation via the degradation of TC-HCl, which is a typical antibiotic residue contaminant usually discharged by pharmaceutical industry, hospital effluent and excretion from humans and livestock. From Fig. 7, for an

adsorption process in the dark, both of the ZnO/C(550N) and Ag/ZnO/C composites exhibited adsorption capacity of almost 40% for TC-HCl, which is much higher than the ZnO(550A) sample (10%). The reason for the high adsorption capacity of TC-HCl by the ZnO/C(550N) and Ag/ZnO/C samples is probably attribute to the strong π-π interactions between the aromatic rings of the antibiotic and the carbonaceous layers which is incorporated in the samples[48, 49] and the relatively higher BET surface area, which was mentioned in Fig. 5 above. Fig. 7 (a) shows the degradation rate of TC-HCl under UV light irradiation without photocatalyst and using the ZnO(550A), ZnO/C(550N) and Ag/ZnO/C composites as the photocatalyst, where C is the concentration of TC-HCl remaining in the solution after irradiation time t, and C_o is the initial concentration of TC-HCl. As can be seen, the self-degradation of TC-HCl (without photocatalyst) was about 9.9% under UV light irradiation for 35 min. It is noteworthy that both ZnO/C(550N) and Ag/ZnO/C composites exhibited significant photocatalytic activities, the degradation rate can reach 90.3% and 95.8% in 35 min under UV light irradiation, respectively, while the degradation rate by ZnO(550A) can only approach 60.1% for the same irradiation time. It reveals that the photocatalytic activity of the composites is improved by hybridizing carbonaceous materials and novel metal Ag in the samples.

Fig. 7 (b) shows the photocatalytic activities of the as-prepared ZnO(550A), ZnO/C(550N) and Ag/ZnO/C composites for degradation of TC-HCl under visible light irradiation. As can be seen, the concentration of TC-HCl has no significant change without catalyst under visible light irradiation for 280 min. Because ZnO has no light adsorption in the visible light region due to its large band gap energy (3.37 eV), the ZnO(550A) sample

exhibited a low photocatalytic activity under visible light irradiation and the degradation rate of TC-HCl is only 15.0% in 280 min. However, by hybridizing carbonaceous layers with ZnO, the ZnO/C(550N) sample could adsorb light in the whole UV-vis region (as shown in Fig. 6 UV/vis DRS). Therefore, ZnO/C(550N) has a good visible-light photocatalytic activity and the degradation rate of TC-HCl reaches 81.0% in 280 min. Moreover, when combining with the SPR effect of Ag, the light absorption intensity of Ag/ZnO/C composites was further enlarged. As a result, the Ag/ZnO/C composites show the best photocatalytic activity and the corresponding degradation rate can reach 90.6% in the same irradiation time. Furthermore, repeated degradation reactions were performed to determine the stability of the Ag/ZnO/C plasmonic photocatalyst. As shown in Fig. 8, the catalyst does not exhibit a significant loss of activity after four consecutive reaction cycles both under UV and visible light irradiation, indicating the outstanding stability of this photocatalyst.

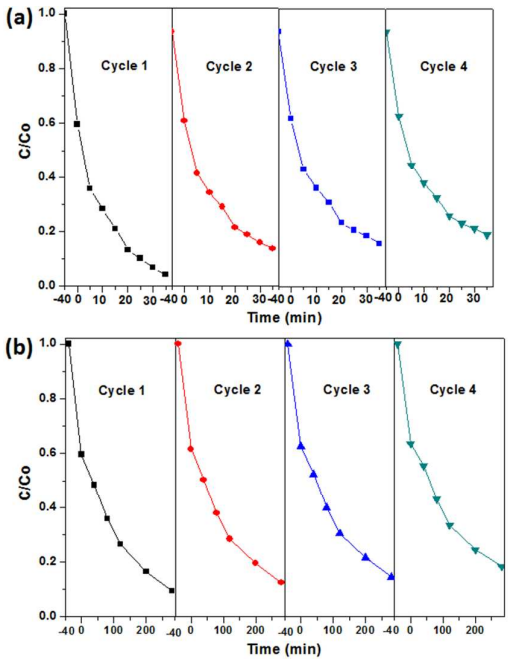

Fig. 8 Four photocatalytic degradation cycles of TC-HCl using Ag/ZnO/C plasmonic photocatalyst: (a) under UV irradiation; (b) under visible light irradiation.

Photocatalytic Mechanism

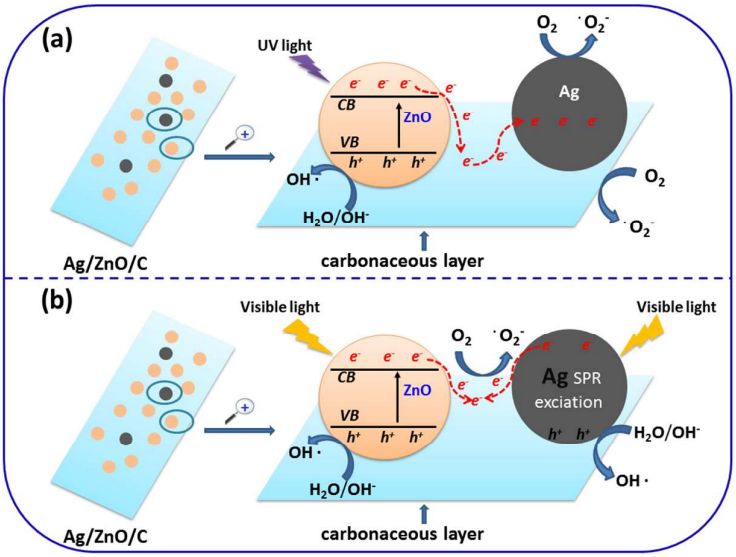

Fig. 9 Proposed photocatalytic mechanisms for degradation of TC-HCl by Ag/ZnO/C composites under (a) UV light irradiation; (b) visible light irradiation.

Based on the characterization and experimental data discussed above, possible photocatalytic mechanisms of the as-prepared Ag/ZnO/C composites under UV and visible light irradiation were proposed and illustrated in Fig. 9. Normally in pure ZnO, photogenerated electrons recombine quickly and only a fraction of the electrons and holes participate in the photocatalytic reaction, resulting in low reactivity.[50, 51] However, when ZnO was modified by carbonaceous layers and Ag, both the UV and visible region of light can be utilized simultaneously. As shown in Fig. 9 (a), under UV light irradiation, electrons (e^-) in the valence band of ZnO were excited to the conduction band with the simultaneous generation of holes (h^+) in the valence band. According to the literature,[52-54] the work function of carbonaceous layers (proposed similar to graphene), Ag and the conduction band (CB) of ZnO are 4.42, 4.7 and - 0.31 eV, respectively. Since the CB of ZnO is smaller than the work function of carbonaceous layers, the photogenerated electrons in the CB of ZnO would

transfer to carbonaceous layers.[55] Besides, a Schottky barrier was formed at the interface of carbonaceous layers and Ag nanoparticles due to the higher work function of Ag than carbonaceous layers, so that the injected electrons on the carbonaceous layers could subsequently move to Ag nanoparticles.[52] Here, in Ag/ZnO/C system, the carbonaceous layers act as electrical paths for the photogenerated electrons from ZnO while Ag nanoparticles act as electron acceptor due to the great electron storage capacity[56] during the UV light driven photocatalysis process. Therefore, the photogenerated electrons and holes were efficiently separated and the lifetime of the excited electrons and holes could be prolonged in the transfer process. Meanwhile, the excess of valence band holes (h^+) left in the ZnO migrated to the surface and reacted with H_2O or OH^- to produce active species such as $OH\cdot$. In addition, photogenerated electrons (e^-) that transferred on the surface of carbonaceous layers and Ag nanoparticles could create more active sites for reaction with O_2 to produce active species $\cdot O_2^-$., synergistically promoting the photocatalytic activity of Ag/ZnO/C composites. The major routes in the photocatalytic TC-HCl degradation mechanism under UV-light irradiation were proposed as follows:

$$ZnO + h\nu \rightarrow ZnO\ (e^- + h^+)$$

$$ZnO\ (e^-) + C \rightarrow ZnO + C\ (e^-)$$

$$C\ (e^-) + Ag \rightarrow C + Ag\ (e^-)$$

$$C\ (e^-) + O_2 \rightarrow C + \cdot O_2^-$$

$$Ag\ (e^-) + O_2 \rightarrow Ag + \cdot O_2^-$$

$$\cdot O_2^- + H_2O \rightarrow OH\cdot + HO_2\cdot$$

$$ZnO\ (h^+) + H_2O \rightarrow OH\cdot + H^+$$

$$\cdot O_2^- + H^+ \rightarrow HO_2\cdot$$

$$2HO_2\cdot \rightarrow H_2O_2 + O_2$$

$$H_2O_2 + \cdot O_2^- \rightarrow OH\cdot + OH^- + O_2$$

$$ZnO\ (h^+) + OH^- \rightarrow ZnO + OH\cdot$$

$$OH\cdot + \text{TC-HCl} \rightarrow \text{degradation products}$$

Furthermore, the separation of photogenerated electrons and holes in the Ag/ZnO/C composites was confirmed by PL emission spectra of ZnO(550A) , ZnO/C(550N) and Ag/ZnO/C composites in Fig. 10. PL emission intensity is related to the recombination rate of excited electron-hole pairs. A lower PL intensity is a general indication of a lower recombination of electron-hole pairs.[57] As can be seen, Ag/ZnO/C composites exhibited the lowest emission intensity among the samples, indicating that the recombination of the photogenerated charge carriers was inhibited greatly in the Ag/ZnO/C composites. The efficient charge separation could increase the lifetime of the photogenerated electrons and holes, accounting for the higher photocatalytic activity of Ag/ZnO/C composites.

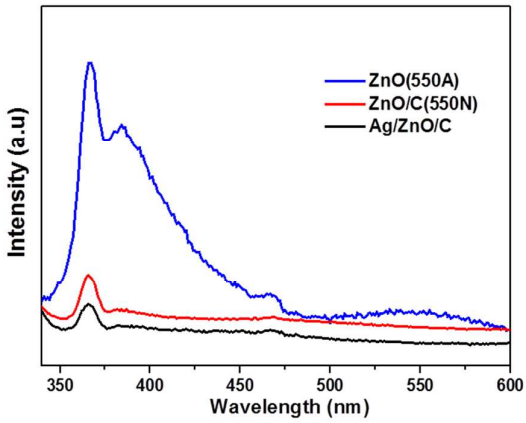

Fig. 10 PL emission spectra of ZnO(550A) , ZnO/C(550N) and Ag/ZnO/C composites.

For the visible light driven photocatalysis process, we illustrated the possible photocatalytic mechanism of the as-prepared Ag/ZnO/C composites in Fig. 9(b). As

mentioned in UV-vis DRS part, pure ZnO had no absorption in the visible light region, while ZnO/C could adsorb light in the whole UV-vis region. This different behavior indicated the hybridized carbonaceous layers are the origin of visible-light absorption and the two components ZnO and C were form a joint electronic system.[58, 59] Combining with the SPR effect of Ag, the light absorption intensity of Ag/ZnO/C composites was further enlarged. Since DRS spectra clearly shows that the optical response of ZnO/C shifts into the visible-light region, under visible light irradiation, ZnO was exicited to form electron-hole pairs,[59, 60] the photogenerated electrons (e^-) then transferred onto the surface of carbonaceous layers. At the same time, the incident visible light was absorbed by the surface plasmon resonance (SPR) of Ag nanoparticles, and a majority of plasmon-excited electrons (hot electrons) generated on the Ag nanoparticles. These hot electrons were energetic enough to transfer onto the carbonaceous layers, leaving behind the hot holes on the Ag nanoparticles. As a consequence, a relative high concentration of photogenerated electrons (e^-) that transferred onto the carbonaceous layers from both of ZnO and Ag could react with O_2 to produce active species $\cdot O_2^-$. Meanwhile, photogenerated holes (h^+) left on the VB of ZnO and the Ag nanoparticles could migrated to the surfaces and reacted with H_2O or OH^- to produce active species such as $OH\cdot$.[32, 61] As we know, the reaction active species such as $\cdot O_2^-$ and $OH\cdot$ produced during the photocatalytic process play an important role and are the mainly reaction species during the degradation of the pollutant. The major routes in the photocatalytic TC-HCl degradation mechanism under visible-light irradiation were proposed as follows:

$$ZnO + h\nu \rightarrow ZnO\ (e^- + h^+)$$

$$ZnO\ (e^-) + C \rightarrow ZnO + C\ (e^-)$$

$$Ag + h\nu \rightarrow Ag\ (e^- + h^+)$$

$$Ag\ (e^-) + C \rightarrow Ag + C\ (e^-)$$

$$C\ (e^-) + O_2 \rightarrow C + \cdot O_2^-$$

$$\cdot O_2^- + H_2O \rightarrow OH\cdot + HO_2\cdot$$

$$ZnO\ (h^+) + H_2O \rightarrow OH\cdot + H^+$$

$$Ag\ (h^+) + H_2O \rightarrow OH\cdot + H^+$$

$$\cdot O_2^- + H^+ \rightarrow HO_2\cdot$$

$$2HO_2\cdot \rightarrow H_2O_2 + O_2$$

$$H_2O_2 + \cdot O_2^- \rightarrow OH\cdot + OH^- + O_2$$

$$ZnO\ (h^+) + OH^- \rightarrow ZnO + OH\cdot$$

$$Ag\ (h^+) + OH^- \rightarrow Ag + OH\cdot$$

$$OH\cdot + TC\text{-}HCl \rightarrow \text{degradation products}$$

By incorporating carbonaceous layers and Ag nanoparticles into the structure to form the Ag/ZnO/C composites, the optical absorption property was improved, the electron-hole pairs' recombination was effectively hindered and the total active reaction sites were increased. As expected, the as-obtained Ag/ZnO/C composites exhibit enhanced photocatalytic activity for the degradation of TC-HCl under visible light.

Conclusions

In summary, Ag/ZnO/C plasmonic photocatalyst was successfully synthesized via a simple calcination and photodeposition method. The ZnO and Ag nanoparticles sized 5-10 nm were evenly and densely distributed on the surface of carbonaceous layers. The synergetic effects

between the excellent optical and photophysics properties of the Ag/ZnO/C structure, which are the capability to utilize both of the UV and visible light, efficient photogenerated electron separation and transportation and the increase of the active reaction sites, all make the resultant photocatalyst exhibit excellent photocatalytic activity towards to TC-HCl degradation. The simple preparation route, low cost and high photocatalytic activity of the sample will greatly promote its practical application to eliminate the organic pollutants from wastewater by utilization of solar energy.

Acknowledgements

The authors are grateful to the financial supports of National Natural Science Foundation of China (Grant No. 21376051, 21306023, 21106017, and 51077013), Natural Science Foundation of Jiangsu (Grant No. BK20131288), Fund Project for Transformation of Scientific and Technological Achievements of Jiangsu Province of China (Grant No. BA2014100).

References

1. M. V. Walter and J. W. Vennes, *Appl. Environ. Microb.*, 1985, **50**, 930-933.

2. K. S. Kim, C. S. Yang and Y. S. Mok, *Chem. Eng. J.*, 2013, **219**, 19-27.

3. C. Liu, V. Nanaboina and G. Korshin, *Chemosphere*, 2012, **86**, 774-782.

4. L. W. Hou, H. Zhang and X. F. Xue, *Sep. Purif. Technol.*, 2012, **84**, 147-152.

5. A. G. Trovo, R. F. P. Nogueira, A. Aguera, A. R. Fernandez-Alba and S. Malato, *Water Res.*, 2011, **45**, 1394-1402.

6. V. Homem, A. Alves and L. Santos, *Sci. Total. Environ.*, 2010, **408**, 6272-6280.

7. X. N. Yu, X. Gao, Z. Y. Lu, X. L. Liu, P. W. Huo, X. L. Liu, D. Wu and Y. S. Yan, *Rsc Adv.*, 2013, **3**, 14807-14813.

8. N. Pugazhenthiran, S. Murugesan, P. Sathishkurnar and S. Anandan, *Chem. Eng. J.*, 2014, **241**, 401-409.

9. M. J. Chen and W. Chu, *J. Hazard. Mater.*, 2012, **219**, 183-189.

10. D. He, Y. B. Sun, L. Xin and J. W. Feng, *Chem. Eng. J.*, 2014, **258**, 18-25.

11. A. B. Djurisic, X. Y. Chen, Y. H. Leung and A. M. C. Ng, *J. Mater. Chem.*, 2012, **22**, 6526-6535.

12. F. Xu, Y. T. Shen, L. T. Sun, H. B. Zeng and Y. N. Lu, *Nanoscale*, 2011, **3**, 5020-5025.

13. G. Williams and P. V. Kamat, *Langmuir*, 2009, **25**, 13869-13873.

14. C. L. Yu, K. Yang, Y. Xie, Q. Z. Fan, J. C. Yu, Q. Shu and C. Y. Wang, *Nanoscale*, 2013, **5**, 2142-2151.

15. A. Mclaren, T. Valdes-Solis, G. Q. Li and S. C. Tsang, *J. Am. Chem. Soc.*, 2009, **131**, 12540-12541.

16. X. Q. Qiu, L. P. Li, J. Zheng, J. J. Liu, X. F. Sun and G. S. Li, *J. Phys. Chem. C.*, 2008, **112**, 12242-12248.

17. X. Q. Qiu, G. S. Li, X. F. Sun, L. P. Li and X. Z. Fu, *Nanotechnology*, 2008, **19**, 215703.

18. J. Bandara, K. Tennakone and P. P. B. Jayatilaka, *Chemosphere*, 2002, **49**, 439-445.

19. Z. C. Wu, C. R. Xu, Y. Q. Wu, H. Yu, Y. Tao, H. Wan and F. Gao, *Crystengcomm*, 2013, **15**, 5994-6002.

20. M. L. Zhang, T. C. An, X. H. Hu, C. Wang, G. Y. Sheng and J. M. Fu, *Appl. Catal. a-Gen.*, 2004, **260**, 215-222.

21. Z. B. Yu, Y. P. Xie, G. Liu, G. Q. Lu, X. L. Ma and H. M. Cheng, *J. Mater. Chem. A*, 2013, **1**, 2773-2776.

22. S. S. Ma, J. J. Xue, Y. M. Zhou and Z. W. Zhang, *J. Mater. Chem. A*, 2014, **2**, 7272-7280.

23. J. B. Mu, C. L. Shao, Z. C. Guo, Z. Y. Zhang, M. Y. Zhang, P. Zhang, B. Chen and Y. C. Liu, *Acs Appl. Mater. Inter.*, 2011, **3**, 590-596.

24. C. Han, M. Q. Yang, B. Weng and Y. J. Xu, *Phys. Chem. Chem. Phys.*, 2014, **16**, 16891-16903.

25. S. S. Ma, J. J. Xue, Y. M. Zhou, Z. W. Zhang and X. Wu, *Crystengcomm*, 2014, **16**, 4478-4484.

26. S. Cho, J. W. Jang, J. S. Lee and K. H. Lee, *Crystengcomm*, 2010, **12**, 3929-3935.

27. Y. Guo, H. S. Wang, C. L. He, L. J. Qiu and X. B. Cao, *Langmuir*, 2009, **25**, 4678-4684.

28. L. Q. Jiang and L. Gao, *Mater. Chem. Phys.*, 2005, **91**, 313-316.

29. J. Khanderi, R. C. Hoffmann, A. Gurlo and J. J. Schneider, *J. Mater. Chem.*, 2009, **19**, 5039-5046.

30. D. G. Yin, L. Zhang, B. H. Liu and M. H. Wu, *J. Nanosci. Nanotechno.*, 2012, **12**, 2248-2253.

31. A. Zielinska-Jurek, E. Kowalska, J. W. Sobczak, W. Lisowski, B. Ohtani and A. Zaleska, *Appl. Catal. B-Environ.*, 2011, **101**, 504-514.

32. W. Y. Gao, M. Q. Wang, C. X. Ran, X. Yao, H. H. Yang, J. Liu, D. L. He and J. B. Bai, *Nanoscale*, 2014, **6**, 5498-5508.

33. J. J. Xue, S. S. Ma, Y. M. Zhou and Z. W. Zhang, *New J. Chem.*, 2014, DOI: 10.1039/C4NJ02004A.

34. Y. P. Zhu, M. Li, Y. L. Liu, T. Z. Ren and Z. Y. Yuan, *J. Phys. Chem. C*, 2014, **118**, 10963-10971.

35. D. K. Mishra, J. Mohapatra, M. K. Sharma, R. Chattarjee, S. K. Singh, S. Varma, S. N.

Behera, S. K. Nayak and P. Entel, *J. Magn. Magn. Mater.*, 2013, **329**, 146-152.

36. K. Kotsis and V. Staemmler, *Phys. Chem. Chem. Phys.*, 2006, **8**, 1490-1498.

37. H. H. Ji, F. Chang, X. F. Hu, W. Qin and J. W. Shen, *Chem. Eng. J.*, 2013, **218**, 183-190.

38. E. Papirer, R. Lacroix, J. B. Donnet, G. Nanse and P. Fioux, *Carbon*, 1995, **33**, 63-72.

39. K. S. W. Sing, D. H. Everett, R. A. W. Haul, L. Moscou, R. A. Pierotti, J. Rouquerol and T. Siemieniewska, *Pure Appl. Chem.*, 1985, **57**, 603-619.

40. H. Pan, J. B. Yi, L. Shen, R. Q. Wu, J. H. Yang, J. Y. Lin, Y. P. Feng, J. Ding, L. H. Van and J. H. Yin, *Phys. Rev. Lett.*, 2007, **99**, 127201.

41. X. P. Sun, S. J. Dong and E. K. Wang, *Macromolecules*, 2004, **37**, 7105-7108.

42. V. G. Pol, D. N. Srivastava, O. Palchik, V. Palchik, M. A. Slifkin, A. M. Weiss and A. Gedanken, *Langmuir*, 2002, **18**, 3352-3357.

43. J. Li and C. Y. Liu, *Eur. J. Inorg. Chem.*, 2010, 1244-1248.

44. N. Zhang, Y. H. Zhang and Y. J. Xu, *Nanoscale*, 2012, **4**, 5792-5813.

45. Y. H. Zhang, Z. R. Tang, X. Z. Fu and Y. J. Xu, *Acs Nano*, 2010, **4**, 7303-7314.

46. C. H. Wu, Y. Z. Zhang, S. Li, H. J. Zheng, H. Wang, J. B. Liu, K. W. Li and H. Yan, *Chem. Eng. J.*, 2011, **178**, 468-474.

47. P. Hu, X. L. Hu, C. J. Chen, D. F. Hou and Y. H. Huang, *Crystengcomm*, 2014, **16**, 649-653.

48. S. J. Yang, J. H. Cho, G. H. Oh, K. S. Nahm and C. R. Park, *Carbon*, 2009, **47**, 1585-1591.

49. Y. C. Hsu, H. C. Lin, C. W. Lue, Y. T. Liao and C. M. Yang, *Appl. Catal. B-Environ.*, 2009, **89**, 309-314.

50. N. P. Xekoukoulotakis, N. Xinidis, M. Chroni, D. Mantzavinos, D. Venieri, E. Hapeshi and D. Fatta-Kassinos, *Catal. Today*, 2010, **151**, 29-33.

51. D. Klauson, M. Krichevskaya, M. Borissova and S. Preis, *Environ. Technol.*, 2010, **31**, 1547-1555.

52. R. Czerw, B. Foley, D. Tekleab, A. Rubio, P. M. Ajayan and D. L. Carroll, *Phys. Rev. B*, 2002, **66**, 033408.

53. Y. Xu and M. A. A. Schoonen, *Am. Mineral.*, 2000, **85**, 543-556.

54. A. L. Giraldo, G. A. Penuela, R. A. Torres-Palma, N. J. Pino, R. A. Palominos and H. D. Mansilla, *Water Res.*, 2010, **44**, 5158-5167.

55. C. X. Guo, H. B. Yang, Z. M. Sheng, Z. S. Lu, Q. L. Song and C. M. Li, *Angew. Chem. Int. Edit.*, 2010, **49**, 3014-3017.

56. S. T. Meyers, J. T. Anderson, C. M. Hung, J. Thompson, J. F. Wager and D. A. Keszler, *J. Am. Chem. Soc.*, 2008, **130**, 17603-17609.

57. Y. F. Chen, W. X. Huang, D. L. He, S. T. Yue and H. Huang, *Acs Appl. Mater. Inter.*, 2014, **6**, 14405-14414.

58. S. W. Liu, C. Li, J. G. Yu and Q. J. Xiang, *Crystengcomm*, 2011, **13**, 2533-2541.

59. L. Zhao, X. F. Chen, X. C. Wang, Y. J. Zhang, W. Wei, Y. H. Sun, M. Antonietti and M. M. Titirici, *Adv. Mater.*, 2010, **22**, 3317-3321.

60. H. Yu, H. C. Zhang, H. Huang, Y. Liu, H. T. Li, H. Ming and Z. H. Kang, *New. J. Chem.*, 2012, **36**, 1031-1035.

61. L. C. Sim, K. H. Leong, S. Ibrahim and P. Saravanan, *J. Mater. Chem. A*, 2014, **2**, 5315-5322.